SOAR: Space Orbiting Advanced Fusion Power Reactor

J.F. Santarius, G.L. Kulcinski, H. Attaya, M.L. Corradini, L.A. El-Guebaly, G.A. Emmert, J.W. Johnson, C.W. Maynard, M.E. Sawan, I.N. Sviatoslavsky, W.F. Vogelsang, P.L. Walstrom, L.J. Wittenberg, and T.E. Luzzi

January 1987

UWFDM-717

Presented at 4th Symposium on Space Nuclear Power Systems, Albuquerque, NM, 12-16 January 1987; Space Nuclear Power Systems 1987 (Orbit, Malabar FL, 1988) 167.

FUSION TECHNOLOGY INSTITUTE

UNIVERSITY OF WISCONSIN

MADISON WISCONSIN

SOAR: Space Orbiting Advanced Fusion Power Reactor

J.F. Santarius, G.L. Kulcinski, H. Attaya, M.L. Corradini, L.A. El-Guebaly, G.A. Emmert, J.W. Johnson, C.W. Maynard, M.E. Sawan, I.N. Sviatoslavsky, W.F. Vogelsang, P.L. Walstrom, L.J. Wittenberg, and T.E. Luzzi

Fusion Technology Institute
University of Wisconsin
1500 Engineering Drive
Madison, WI 53706

http://fti.neep.wisc.edu

January 1987

UWFDM-717

Presented at 4th Symposium on Space Nuclear Power Systems, Albuquerque, NM, 12-16 January 1987; Space Nuclear Power Systems 1987 (Orbit, Malabar FL, 1988) 167.

SOAR: SPACE ORBITING ADVANCED FUSION POWER REACTOR

J.F. Santarius, G.L. Kulcinski, H.M. Attaya, M.L. Corradini,
L.A. El-Guebaly, G.A. Emmert, J.W. Johnson, C.W. Maynard, M.E. Sawan,
I.N. Sviatoslavsky, W.F. Vogelsang, P.L. Walstrom, and L.J. Wittenberg

Fusion Technology Institute
1500 Johnson Drive
University of Wisconsin-Madison
Madison, Wisconsin 53706

T.E. Luzzi

Grumman Corporation, M/S A-08-35
Bethpage, NY 11714

January 1987

UWFDM-717

Presented at 4th Symposium on Space Nuclear Power Systems, Albuquerque, NM, 12-16 January 1987.

SOAR: SPACE ORBITING ADVANCED FUSION POWER REACTOR

J.F. Santarius, G.L. Kulcinski, H.M. Attaya, M.L. Corradini,
L.A. El-Guebaly, G.A. Emmert, J.W. Johnson, C.W. Maynard, M.E. Sawan,
I.N. Sviatoslavsky, W.F. Vogelsang, P.L. Walstrom, and L.J. Wittenberg
Fusion Technology Institute
University of Wisconsin-Madison
1500 Johnson Drive
Madison, WI 53706-1687

T.E. Luzzi
Grumman Corporation, M/S A-08-35
Bethpage, NY 11714

ABSTRACT

The Space Orbiting Advanced Fusion Power Reactor (SOAR) is designed to deliver up to 1000 MWe for at least 600 s from a D-^{3}He plasma. About 96% of the fusion energy is in charged particles, and much of this energy is electrostatically converted directly into electricity at high efficiency (~ 85%). Advanced shield design allows SOAR to deliver approximately 2 kilowatts of electricity for every kilogram of material orbited. The SOAR reactor concept is designed to allow rapid startup and shutdown procedures. The lack of radioactivity on launch and the low radioactive inventory after operation make the SOAR concept attractive from maintenance, safety and environmental perspectives. The plasma physics approach extrapolates from the present plasma physics and fusion technology knowledge base using concepts which can be tested on existing or near-term devices. The symbiosis of burst mode requirements, D-^{3}He tandem mirror fusion reactor characteristics, and the space environment leads to a very high performance design concept.

INTRODUCTION

Fusion reactors based on the deuterium/helium-3 (D-^{3}He) reaction are efficient for space burst mode power because:

- Sufficient terrestrial ^{3}He reserves exist for the use of "low-neutron" D-^{3}He fuel;
- Radiation shielding mass is reduced;
- Radiators can be eliminated by dissipating waste heat adiabatically in the shield;
- Highly efficient direct electrostatic conversion of energy to electricity by the use of low mass direct converters is possible;
- Vacuum pumping and cryogenic cooling systems are reduced in mass and complexity;
- SOAR is nonradioactive until operated;
- No "criticality" potential exists during a launch phase accident;
- Low radioactivity and afterheat levels are induced during operation and only short half life isotopes remain for waste disposal; and
- Response from cold start is rapid (~ 10 seconds).

D-^{3}He fusion reactors for use in space (Englert 1962) and on earth (Miley 1976, Dawson 1981, Wittenberg et al. 1986) have been under investigation for some time.

Our calculations indicate that a tandem mirror magnetic confinement device would make the most efficient use of this advanced fuel. The main reasons for this are the possibility of electrostatic direct conversion and the ease of increasing magnetic fields to maintain plasma pressure. The general configuration for 250 MWe and 1000 MWe versions of SOAR is indicated in Figure 1,

where the space shuttle is also shown for comparison. Other concepts such as toroidal fusion reactors or inertial confinement (laser or ion beam driven) fusion reactors have been considered, but preliminary estimates of the mass utilization favor the tandem mirror.

At this time, the SOAR study is primarily aimed at critical issues and, since it was only recently begun, not all of the details of the design are self-consistent. The intent of this phase of the SOAR study is to identify areas requiring more intense work, to calculate masses, and to define mass scaling laws sufficient for an approximate estimate of the attainable power to mass ratio at a given power level. A nominal reference case, based on a power level of 1000 MWe and a 600 s operation time, has also been generated in order to define characteristic parameters. Some selected parameters are given in Table 1.

PLASMA PHYSICS AND ENGINEERING

The key advantage that a D-^{3}He fusion reactor has over both fission reactors and deuterium/tritium(D/T)-fueled fusion reactors is that almost all of the energy generated by the nuclear reactions is in the form of charged particles. Besides reducing the mass required for neutron shielding, this potentially allows direct electrostatic conversion of charged particle energy to electricity at efficiencies much higher than attainable through a Carnot cycle. The percentage of fusion reaction energy in charged particles for the three main fusion reactions is shown in Figure 2. These reactions are:

$D + T \rightarrow {}^4He(3.5\ MeV) + n(14.1\ MeV)$

$D + {}^3He \rightarrow {}^4He(3.6\ MeV) + p(14.7\ MeV)$

$D + D \rightarrow {}^3He(0.82\ MeV) + n(2.45\ MeV)$ 50%

$D + D \rightarrow T(1.01\ MeV) + p(3.02\ MeV)$ 50%

For typical SOAR parameters, less than 5% of the fusion energy is carried by neutrons.

Fusion power reactor designs based on the $^3He(d,p)\alpha$ reaction have been less intensely studied than those based on the $t(d,n)\alpha$, $d(d,n)^3He$, and $d(d,p)t$ reactions due to the scarcity of ^3He on Earth. However, sufficient ^3He for a 1000 MWe SOAR reactor, operating for 10 minutes, would cost $\leq$ $7000 (Wittenberg et al. 1986 and 1987). The generic advantage of reduced neutron shielding requirements applies to any magnetic confinement concept, but direct conversion is most readily utilized in an open field line geometry. Therefore, the tandem mirror configuration has been chosen for the initial SOAR reference case.

A tandem mirror fusion reactor is essentially a linear magnetic bottle in which plasma end loss is reduced by a combination of magnetic fields ("magnetic mirrors") and electrostatic potentials. The potentials are maintained by creating non-Maxwellian populations of ions through neutral beam (NB) injection and of electrons through electron cyclotron range of frequencies (ECRF) heating (Baldwin and Logan 1979, Kesner et al. 1984, and Perkins et al. 1985). The fusion power is produced in the central cell region by nearly Maxwellian populations of deuterium and helium-3 ions. The thermal barrier region serves to thermally insulate the central cell from the plug region.

This allows ion end loss to be reduced through a linear dependence of the plug electrostatic potential on electron temperature rather than through a logarithmic dependence on density. The core plasma is surrounded by a low density, low temperature halo plasma which pumps away impurities due to wall outgassing or other neutral gas sources.

Stable, axisymmetric operation is assumed to be maintained in SOAR by allotting a substantial power (25 MW absorbed) to central cell ion cyclotron range of frequencies (ICRF) heating. Three main methods of achieving axisymmetry are presently under investigation: RF stabilization (Hershkowitz et al. 1985), wall stabilization (Berk et al. 1984), and magnetic limiter stabilization (Kesner et al. 1985). Although a substantial theoretical effort in each area is in progress, the critical issues involved will require high power and high density experiments for their resolution.

The SOAR plasma is modelled using standard thermal barrier tandem mirror reactor theory (Logan et al. 1984 and 1987), suitably modified for the D-^{3}He fuel cycle. In addition, a new operating mode is examined--in which the fusion product protons not needed to sustain plasma losses are caused to scatter nonadiabatically and to be lost out the ends on a time scale short compared to the time it would take them to deposit their energy in the core plasma (Santarius 1987). The resulting, narrow energy spectrum of the proton end loss stream should lead potentially to a high direct converter efficiency (> 80%), although the details of the energy spread remain to be calculated. This new mode is a desirable, but not necessary, feature of a D-^{3}He tandem mirror reactor design. The option of allowing the fusion products to slow

down in the core plasma is also under investigation; this would mitigate the difficulties of designing a high voltage direct converter. A tandem mirror reactor computer code, PBAFTM, has been written to solve the particle and power balance equations involved and to assess the performance of SOAR. Using simple mass scaling laws generated in the course of this study for the most important components of SOAR, the reactor parameters were optimized for power per mass over a space of 21 variables. The axial dependence of magnetic field magnitude, electrostatic potential, and densities for the preliminary reference case is shown in Figure 3. Reference case plasma physics parameters for a 1000 MWe version of SOAR are given in Table 2.

MAGNETICS AND CRYOGENICS

The 1000 MWe reference case has a central cell, on-axis field of 7.7 T, 18 T choke coils at each end of the central cell, and 12 T end coils outside of the choke coils. The parameters for the magnet system are given in Table 3; an isometric view of the winding pack envelopes is given in Figure 4. All coils in the system are axisymmetric solenoids.

Choice of Central Cell Magnet Technology

The nominal SOAR operating scenario is a single 600 s burn. Use of both resistive (liquid hydrogen-cooled aluminum) and superconducting windings was considered, since steady state operation is not required. With resistive coils, the I^2R power is to some degree offset by the greater heat of vaporization of the coolant (H_2 vs. He) and reduced nuclear shield mass. The final consideration in choosing superconducting coils was the fact that superconducting coils can be kept energized in persistent mode indefinitely before

startup with negligible energy expenditure by use of demountable current leads; resistive coils cannot be energized until immediately before startup because of steady-state power consumption. The combination of central cell energy storage requirements (6200 MJ), the need for a startup power supply capable of energizing the coils in 60 s or less, and the additional power conversion equipment for supplying I^2R power during the burn make the total mass of the resistive coil option considerably larger than the superconducting option.

Various options for cooling the windings were considered. The simplest approach is cooling with stagnant pressurized superfluid helium (He II). In all of the approaches considered, a small refrigerator/liquefier is provided to handle standby (reactor off) heat loads due to conduction and thermal radiation. Nuclear heating loads during the plasma burn are much greater and are absorbed by single-phase heating and/or vaporization of liquid helium. Nuclear heat during operation is conducted radially outward through cooling passages in the windings to a reservoir outside of the windings. The drawback to the above approach is that the specific cooling capacity available is the enthalpy change for single-phase heating between about 1.5 and 2.0 K, namely 1.4 kJ/kg.

The remaining options, listed below, all involve evaporation of liquid helium, in order to take advantage of the enthalpy difference of about 20 kJ/kg between the liquid and vapor phases. They are:

1. Windings with boiling He I or He II and artificial gravity for phase separation;

2. Open-loop He I-cooled force-flow conductor with pumped two-phase helium;
3. Single-phase force-flow conductor with pump and evaporative heat exchanger; and
4. Pressurized He II in windings with evaporative He II heat exchanger.

Option 1 was eliminated because of complications in system design caused by spinning the entire reactor around the central cell axis in order to provide artificial gravity. Option 3 was eliminated because of the mass of a second pump and heat exchanger required; one pump is needed for the primary loop and a second for supply of the heat exchanger. In comparing the remaining two options, option 2 is preferable because a He II heat exchanger is very massive. In all of the evaporation modes considered, a high-capacity liquid acquisition system to ensure supply of the liquid phase only to the pump is needed.

All of the evaporative modes require discharge during the 600 s of operation of large quantities (~ 80 tonnes) of cold helium vapor into space or into cooling systems for beams or other applications. If dumped directly into space, the resultant helium concentration is a potential problem for reactor operation because of possible electrical breakdown in the direct converter and contamination of the plasma. In order to estimate helium concentration near the reactor, an analytic solution to helium flow for the spherically symmetric, irrotational case was obtained. For a mass efflux rate of 100 kg/s, the helium concentration at a point 100 m distant from the source is about 10^{22} particles/m^2. These levels are probably too high to be acceptable. However, preliminary estimates indicate that with directed ducting of the

vapor and use of shrouds around critical system components, the above figure can be reduced by three orders of magnitude or more, i.e. to acceptable levels.

Choke Coils

The most advanced components of the magnet system are the two high-field, superconducting choke coils. The windings are cooled by He II conduction; superfluid temperature is needed because of the extremely high peak field (20.2 T) in the winding pack. In the present design, magnetic stresses are carried by graphite-epoxy composite interleaved with the conductor. The major technical problems are the relatively low transverse modulus and strength of the composite and the mismatch in thermal contraction between the composite and the Nb_3Sn/Cu conductor. Possible approaches to solving the thermal contraction problem are winding under tension in order to put the conductor under compression at room temperature or winding at low temperature. The most satisfactory solution would be use of a composite with compatible thermal contraction behavior.

MAGNET SHIELDING

SOAR requires an efficient and lightweight shield to protect the superconducting magnet against neutrons and neutron-induced gamma-rays. A brief summary of the work done is mentioned here and the reader is referred to El-Guebaly (1987) for more thorough coverage of the shielding design. Due to the short operation time of SOAR, the concern is not radiation damage to the superconducting magnet but is the difficulty of nuclear heat rejection from the 4.2 K magnet. In order to reduce the helium coolant mass required to remove this

heat from the magnet, shields must be used to drop the heat by several orders of magnitude. Many shielding, structural, and coolant materials have been evaluated to assess their shielding capability. LiH was found to be the best shielding material that meets the combined criteria of highly efficient and lightweight shield. The structure and coolant constitute a small fraction of the shield volume and calculations show that they have no significant effect on magnet heating. Therefore, the choice between them should be based on other aspects such as mechanical design, thermal hydraulics, material compatibility, strength and stress limitations.

A shield thickness optimization study was performed in which the total mass of the central cell was minimized. This included the mass of the shield, superconducting magnet, and magnet He coolant. Figure 5 indicates that the minimum central cell mass is ~ 300 tonnes. This corresponds to a LiH shield thickness of 0.35 m and a peak nuclear heating in the magnet of 23 kW/m^3. Similarly, the total mass for the shield, magnets, and He coolant in the end cells is ~ 100 tonnes.

HEAT DISSIPATION IN THE SOAR REACTOR

Heat dissipation in space has always been a challenging problem and continues to be a major subject for investigators. Basically, there are two ways to manage heat in space; the first is to radiate it away and the second is to absorb it adiabatically. Heat dissipation by radiation is the most commonly used method in space and is the only viable method for long term steady-state dissipation. It takes the form of rather bulky and heavy radiators which are vulnerable to meteroid damage, as well as more innovative but unproven schemes

such as dust column, liquid droplet, and liquid belt radiators. Adiabatic heatup is only viable for systems, such as SOAR, with a short term burst mode of operation. The shield materials presently considered for SOAR, LiH and Li, also have the requisite characteristic needed for adiabatic heatup, namely a high specific heat. Additionally, they are of low density, have a low vapor pressure, are stable, are compatible with structural materials, and undergo a phase change which can be put to advantage for absorbing heat. These materials can, therefore, double as shields and as heat absorbers. Table 4 gives the pertinent properties of LiH and Li.

The D-^{3}He reaction produces a very high ($\leq$ 1.6 MW/m^2) surface heat load on the first wall, and this heat must be spread out in the shield for this scheme to work. Unfortunately, no material has a high enough thermal conductivity to be able to do this in 600 s without exceeding the melting temperature of the first wall. The heat distribution method we have adopted is a circulating He gas which uses the first wall as a heat source and the bulk shield as the sink. Thus, the first wall consists of a bank of tubes through which the He gas flows and absorbs the surface heat. From there the gas circulates through the shield in tubes immersed in the shielding material. Figure 6 shows a section of the central cell with the plasma in the center, surrounded by the shield and the magnet. The arrows show the flow distribution of the He gas. Gas circulators are strategically located along the central cell with the motors outside the magnet.

LiH is the best shield from the standpoint of minimization of mass. The melting temperature of LiH is 960 K and its heat of fusion is 2770 kJ/kg.

Its primary drawbacks are a low thermal conductivity and a high expansion upon melting. The best way to use it would be below the melting point. However, it will be very difficult to prevent melting at some localized hot spots. The two primary structural material candidates are Mo and Nb alloys with a slight preference for the Nb alloy. Both have high strength at elevated temperatures up to ~ 1600 K and have a low thermal stress coefficient. The Nb alloy, however, is more easily fabricated and is much more ductile over the whole operating temperature range.

In summary, an adiabatic heatup shield can be designed for SOAR, using LiH as the primary shield material, Nb alloy as the structure and circulating He gas as a means of distributing the heat. Table 1 gives some preliminary parameters for the SOAR reference case. The burn is assumed to last for 600 s and the ambient temperature to be 200 K. The average temperature of the shield reaches 808 K, well below its melting point.

DIRECT CONVERTER

An electrostatic direct converter is used at one end of SOAR to convert the directed kinetic energy of particles streaming out the end of the reactor into high voltage DC power. By careful control of the mirror ratio at the two ends of the central cell and of the electrostatic potential in the two end plugs, most of the ion end loss can be directed out one end of the reactor. The electrons are directed out the other end by biasing the opposite end wall slightly positive relative to the ground potential at the entrance to the direct converter.

The current and power of the various energy groups of ions entering the direct converter for the reference case are shown in Table 5. The 15.2 MeV protons are those protons which were born at 14.7 MeV and scattered nonadiabatically into the loss-cone before slowing down. They acquired an additional 0.5 MeV energy because of the positive potential of the central cell. The lower energy components consist of the end loss of fuel ions, fusion-born alpha particles, and thermalized protons. Because of the energy spectrum, a "venetian blind" direct converter (Moir and Barr 1973, Barr and Moir 1983) with at least 2 or 3 stages is desirable to achieve high efficiency. In this paper, we present results from a preliminary study of a 2 stage direct converter; a 3 stage direct converter is also being considered.

The SOAR 2 stage direct converter collects the energetic protons at high voltage (13 MV) and the other groups at lower voltage (1.3 MV). A schematic of a 2 stage converter is shown in Figure 7. The entrance grid sets the ground potential; the electron suppressor grid repels any electrons entering the direct converter so they do not get accelerated to 13 MeV and degrade the net collected current. The grids will be heated because they intercept a fraction of the incident ion flux.

Six cooling concepts were examined for the suppressor grid. The lightest mass concept was chosen for the baseline design. The first employs liquid-cooled swirl tubes where the water is discarded during power generation. In swirl tubes the water is forced to flow in a helical pattern through a circular tube. The mechanism of surface boiling with bubble recondensation in the subcooled liquid near the tube center results in an extremely high heat

transfer device. In calculating the mass only the water was considered. The second concept employs swirl tubes with cooled and recirculating water. In this concept only the weight of the coolant water radiator is considered. Radiation from the radiator surface at the relatively low coolant temperature is the dominant heat conductance used to calculate the required heat transfer surface area and hence the weight of the radiator. The third concept employs forced circulation boiling liquid heat transfer. The water is recirculated through a radiator. The required radiator surface area is large due to the poor steam condensation heat conductance. Only the mass of the radiator is considered. The fourth concept employs high pressure and velocity recirculating gaseous coolant. The pressure is 140 atmospheres. Radiation from the radiator determines its size. Only the mass of the radiator is considered. The fifth concept employs the melting, during power generation, of a solid lithium mass contained within the grid tubes. Only the mass of the lithium is considered. The sixth concept employs direct radiation from the grid element itself, and three materials were considered. The mass is that of the grid element. Table 6 shows the six concepts and their masses. The lightest mass concept is the last, the radiating grid, and it was chosen for the baseline design. Since only a part of the system mass of the other concepts was considered, their actual masses will be greater than that shown.

Three radiative grid materials were considered, carbon, TZM, and tantalum. Carbon is in the form of a carbon-carbon composite. TZM is a molybdenum alloy containing small amounts of titanium and zirconium. The carbon grid diameter is 10 mm and the TZM and tantalum grid diameters are 3 mm. The power into the direct converter is 1288 MW. Table 7 shows the suppressor grid diameter and

mass for the three grid materials radiating between 1400 and 2000 C. Also shown is the thermionic emission current and the power loss. The grid diameter is determined from the heat flux for the material and radiating temperature and the power load onto the grid. The thermionic emission current is determined for the grid material and its radiation temperature. The power loss occurs because the emitted electron current flows from the grids to the high voltage collector and reduces the net collected current. The two factors in the choice of a radiating grid are the mass and power loss. Table 7 shows that the carbon grid at 1400 C has the lowest thermionic current and a mass of 3.2 tonnes. The carbon grid at 1600 C has a slightly lower mass, but the thermionic current is excessive. The carbon suppressor grid at 1400 C with a diameter of 65.5 m and mass of 3.2 tonnes, respectively, is chosen for the baseline design. Sputtering of the carbon grid during the power cycle time is negligible.

The ion collectors are designed of lightweight tantalum foil supported by a structural frame that is shielded from the ion flow. The foil is 0.13 mm thick. Tantalum foil as low as 8 μm is commercially available. The diameter of the collectors is assumed to be the same as the suppressor grid. Sputtering of the tantalum foil during the power cycle time is negligible. Table 8 shows the masses of the grids, collectors, and structural supports for the ion end of the reactor. In addition to thermionic emission, other loss mechanisms include secondary electron emission, finite opacity of the grids and low voltage collector, ion-neutral scattering in the direct converter, and the finite kinetic energy at which ions strike the collectors. The high voltage collector receives 52 A of current and 689 MW of power. The low voltage collector

gathers 174 A and 226 MW. The electron suppressor grid receives 9 A and 5 MW. The net power output for the 1000 MW (nominal) case is estimated to be 910 MW, which gives an overall direct converter efficiency of 71%. This is based on a grid transparency of 99% and a "venetian blind" transparency of 95%. The lower transparency of the "venetian blinds" arises from the finite angular spread of the incident ions. A 3 stage direct converter in which the high energy protons are collected at two voltages might achieve a somewhat higher efficiency. The plasma parameter optimization assumes an overall direct converter efficiency of 78%. This value depends strongly on the energy spread of the nonadiabatic proton loss stream--a quantity which is presently being calculated.

POWER HANDLING

The high voltage electrical energy from the direct converter must be converted to levels suitable for distribution and for powering equipment. The detailed load requirements for SOAR have not yet been defined, and the possibility of using this energy at megavolt levels is under consideration. If the power must be used at lower voltages, several options exist.

A belt or chain driven electrostatic particle accelerator may be made to operate in the reverse mode, i.e. rather than drive the chain to carry charge to the terminal, the charge on the terminal may be used to drive the chain and thus power a conventional generator. There are two problems related to applying this approach to the present design. The first problem is that present chain design is such that only small currents may be carried by the chain. To use this technique would require an increase in current carrying capacity of

between 4 and 5 orders of magnitude. The second problem, which may be of concern for any concept, is the difficulty of holding 13 MV in a vacuum. To stand off voltages this high outside the terminal in the region of the charging chain, the space between the terminal and the tank is filled with SF_6 at about $5x10^5$ Pa pressure. To prevent arcing inside the accelerating column, which is in vacuum, a set of corona rings is established to carefully control the potential gradient and thus avoid gross breakdown and arcing. Since the causes and factors affecting this kind of breakdown in vacuum are not understood, an experiment and analytical study will be required.

Another technique in present use for the conversion of high voltage DC uses inverters based on switched thyristors. Since any alternating current system will require transformers and the attendant mass of the transformer core, to keep the system mass as low as possible the frequency of the system would be kept as high as possible--no less than 400 Hz and possibly greater than 1000 Hz. The present status of thyristor development limits the voltage across one thyristor to about 5 kV. Since all of these inverting units are in series, any failure in switching one of them could result in the full 14 MV appearing across one inverter. Thus the inverting units must be carefully matched and a protection scheme devised to prevent catastrophic failure in the event of a momentary fault. Since it may not be feasible to connect the inverters as one large series unit producing 13 MV AC to be reduced to a lower voltage via transformers, the inverting units would be connected in a series-parallel fashion to provide several sources of alternating current at 200-300 kV. These sources could be coupled together via transformers to form the main power output. However, since the inverter sections run as high as 13 MV, the

primary-to-secondary insulation on the transformers must withstand the voltage. This might be avoided by using each inverter to drive a motor-generator set. In this case the motor-generator shaft could be used to stand off the voltage. The complication would be the added mass and complexity of a rotating system.

Until load requirements are specified, our primary emphasis is on collecting the power at high voltage. Nevertheless, various aspects of the power handling system are under investigation. These areas include: feasibility of improving thyristor performance, system mass, system efficiency and rejection of waste heat, network stability, ability of the source to follow the load and, failure modes and consequences. At the present time some variant of the solid state inverter scheme seems to be the choice to pursue for further investigation. However, it is possible that other more promising techniques may be found.

CONCLUSIONS

We have identified an attractive power station option for space burst mode power: the SOAR D-^{3}He tandem mirror fusion reactor. The symbiosis of burst mode requirements, D-^{3}He fusion reactor characteristics, and the space environment has led to large improvements over earthbound fusion reactor concepts. In particular, a mass utilization of ~ 2 kWe/kg-orbited is attained, radioactivity is absent at launch, and fuel costs are small. Key features of SOAR include the use of D-^{3}He neutron-lean fuel, blow-through magnet cooling, and direct converters. The technology extrapolation required for SOAR appears to

be reasonable, and the plasma analysis has led to plausible parameters. The mass utilization of SOAR is very attractive for space applications.

ACKNOWLEDGMENT

The authors wish to acknowledge helpful discussions with Dr. Jerry Parmer from General Dynamics. This work was supported under Air Force contract F33615-86-C-2705 and by the Grainger Foundation.

TABLE 1. Preliminary SOAR Machine and Power Parameters.

Mass utilization	~ 2 kWe/kg
Fusion power	1900 MW
Net power	1000 MWe
Net efficiency	53 %
Recirculating power	10 %
Total mass	~ 500 tonnes
Central cell first wall radius	0.63 m
First wall surface heat load	1.6 MW/m^2
Energy dissipated in shield	342 GJ
Shield thickness	0.36 m
Mass of LiH	94 tonnes
Initial shield temperature	200 K
Final average shield temperature	808 K

TABLE 2. Preliminary SOAR Plasma Parameters.

Fusion power	1900 MW
Percent of fusion power in nonadiabatic protons	53%
Percent of fusion power in neutrons	3.6%
Central cell ICRF heating power	25 MW
End cell heating power	45 MW
Bremsstrahlung and synchrotron radiation	470 MW
Central cell (power producing region)	
^{3}He to D density ratio	1.4
Plasma radius	0.55 m
Length	73 m
On-axis magnetic field	7.7 T
Ion temperature	119 keV
Electron temperature	91 keV
Electron density	8×10^{20} m^{-3}
Volume-averaged beta (plasma pressure/magnetic field pressure)	0.6
End cell lengths	6 m

TABLE 3. Preliminary SOAR Magnet Parameters.

Central Cell	
Module length	3.05 m
No. of modules	24
On-axis field	7.7 T
Peak field	7.8 T
Total stored energy	6200 MJ
Winding pack inner radius	1.07 m
Winding pack thickness	62 mm
Conductor type	NbTi/Cu/Al
Cooling method	2-phase He I force-flow
Choke Coils	
Winding pack length	2.3 m
On-axis field	18.0 T
Peak field	20.2 T
Winding pack inner radius	1.0 m
Winding pack thickness	0.41 m
Conductor type	
- grades I and II	Nb_3Sn/Cu
- grade II	NbTi/Cu
Cooling method	Pressurized stagnant He II

TABLE 4. Pertinent Properties of LiH and Li for the Shield Adiabatic Heatup Calculations.

	Temp. (K)	LiH	Li
Specific heat (kJ/kg K)	200-300	3.75	2.9
	300-500	4.60	3.9
	500-800	6.05	4.3
Melting temp. (K)		960	453
Heat of fusion (kJ/kg)		2770	433
Thermal conductivity (W/mK)	470	4.4	44
	620	4.1	47
Vapor pressure (torr)	900	6.7×10^{-2}	7.6×10^{-2}
Density (kg/m^3)	solid	780	530
	liquid	550	520

TABLE 5. Energy Spectrum Entering Direct Converter.

	Species	Current (A)	Energy per Charge (MeV)	Power (MW)
High voltage	p	68	15.2	1039
Low voltage	d	1.2	3.1	4
	α	4.0	2.6	4
	d	134	1.4	192
	p	22	1.4	31
	^3He	6.3	1.4	9
	α	0.2	1.4	0.3
	e	46	0.2	9
		235 A of ions		1288 MW of ions

TABLE 6. The Six Direct Converter Suppressor Grid Cooling Concepts and Their Masses.

Concept	Mass (tonnes)
1. Surface boiling swirl tubes--discard water	1540
2. Swirl tubes	670
3. Forced circulation boiling liquid coolant radiative heat rejection	2×10^6
4. Gaseous coolant radiative heat rejection	86
5. Solid lithium melting	89
6. Radiative grid	3.2

TABLE 7. Suppressor Grid Diameter and Mass for the Three Grid Materials Radiating between 1400 and 2000 C.

Material	Grid Temp. (C)	Diameter (m)	Mass (tonnes)	Thermionic Emission Current (A)
Carbon	1400	65.5	3.2	24
	1600	52	2.0	370
TZM	1400	122	34	47
	1800	79	14	11400
	2000	66	10	84000
Tantalum	1400	113	25	470
	1800	74	11	71000
	2000	61	7	437000

TABLE 8. Masses of the Grids, Collectors, and Structural Supports for the Ion End Direct Converter of SOAR.

Component	Mass (tonnes)
Entrance grid	3.2
Suppressor grid	3.2
Low voltage collector	7.1
High voltage collector	7.1
Structural supports	5
Total	25.4

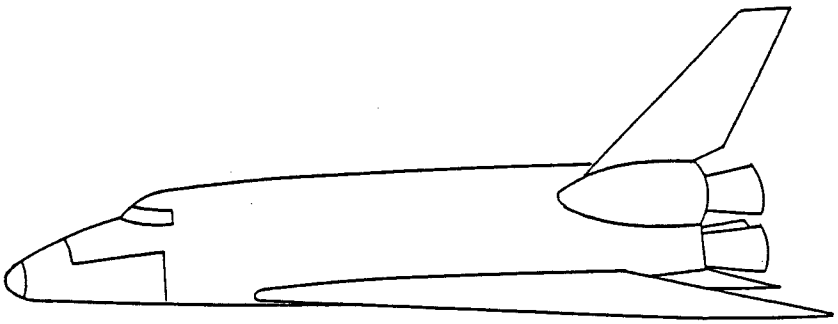

250 MW

1000 MW

FIGURE 1. General Configuration of 250 MWe and 1000 MWe Versions of SOAR. The Space Shuttle is Shown for Comparison.

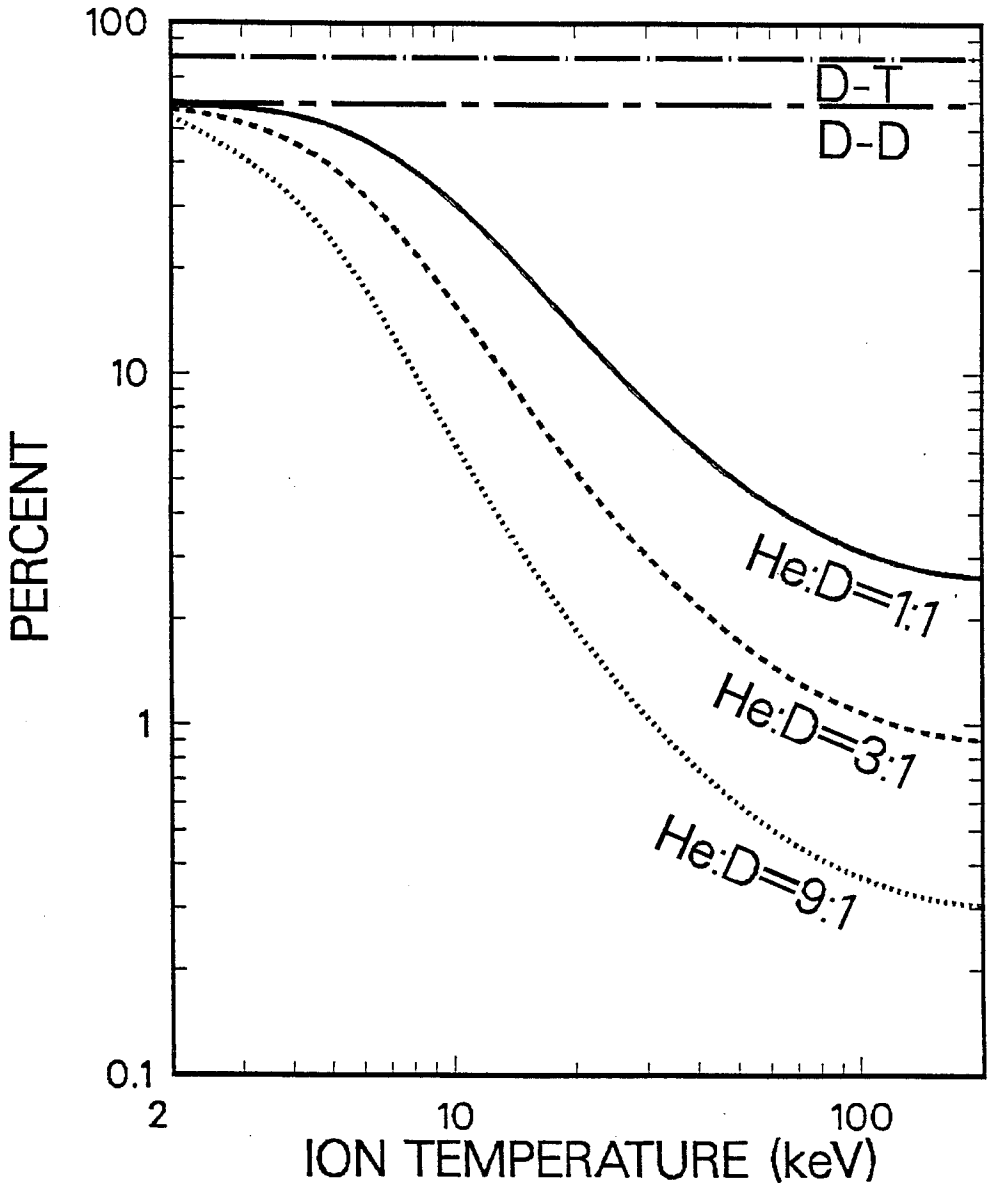

FIGURE 2. Percentage of Fusion Reaction Energy in Charged Particles for the Three Main Fusion Reactions.

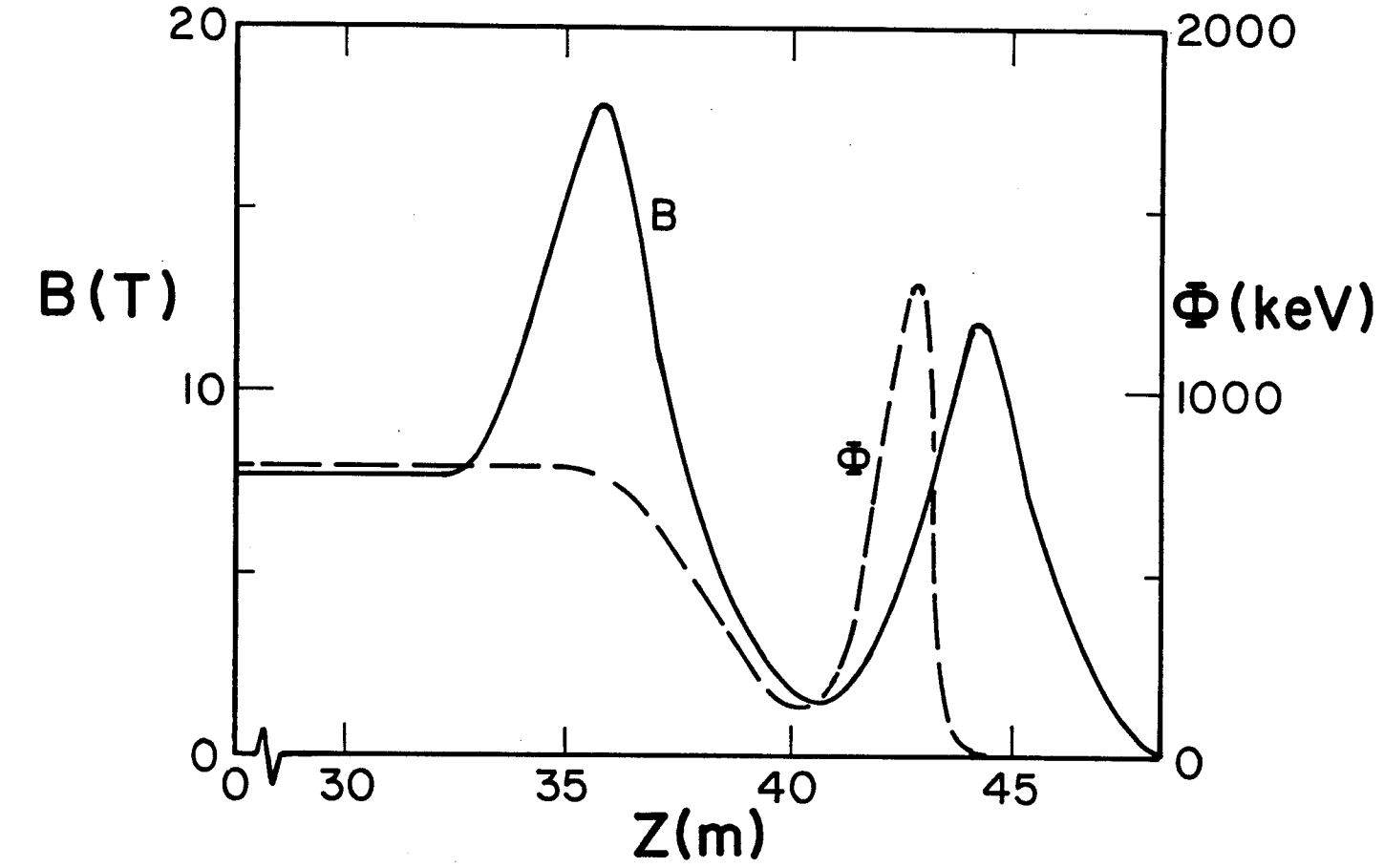

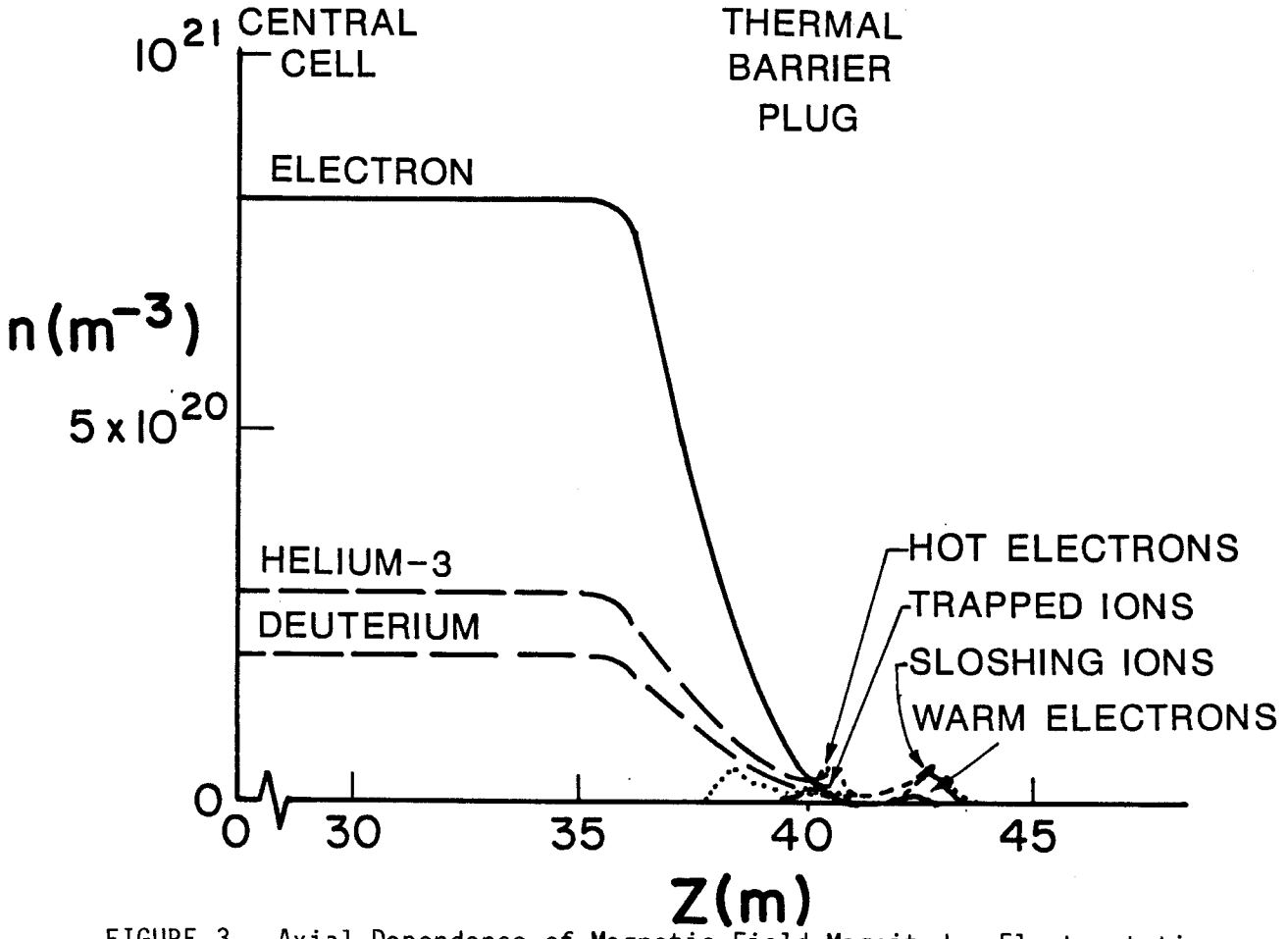

FIGURE 3. Axial Dependence of Magnetic Field Magnitude, Electrostatic Potential, and Densities for the Preliminary Reference Case.

FIGURE 4. Isometric View of the SOAR Magnet Winding Pack Envelopes.

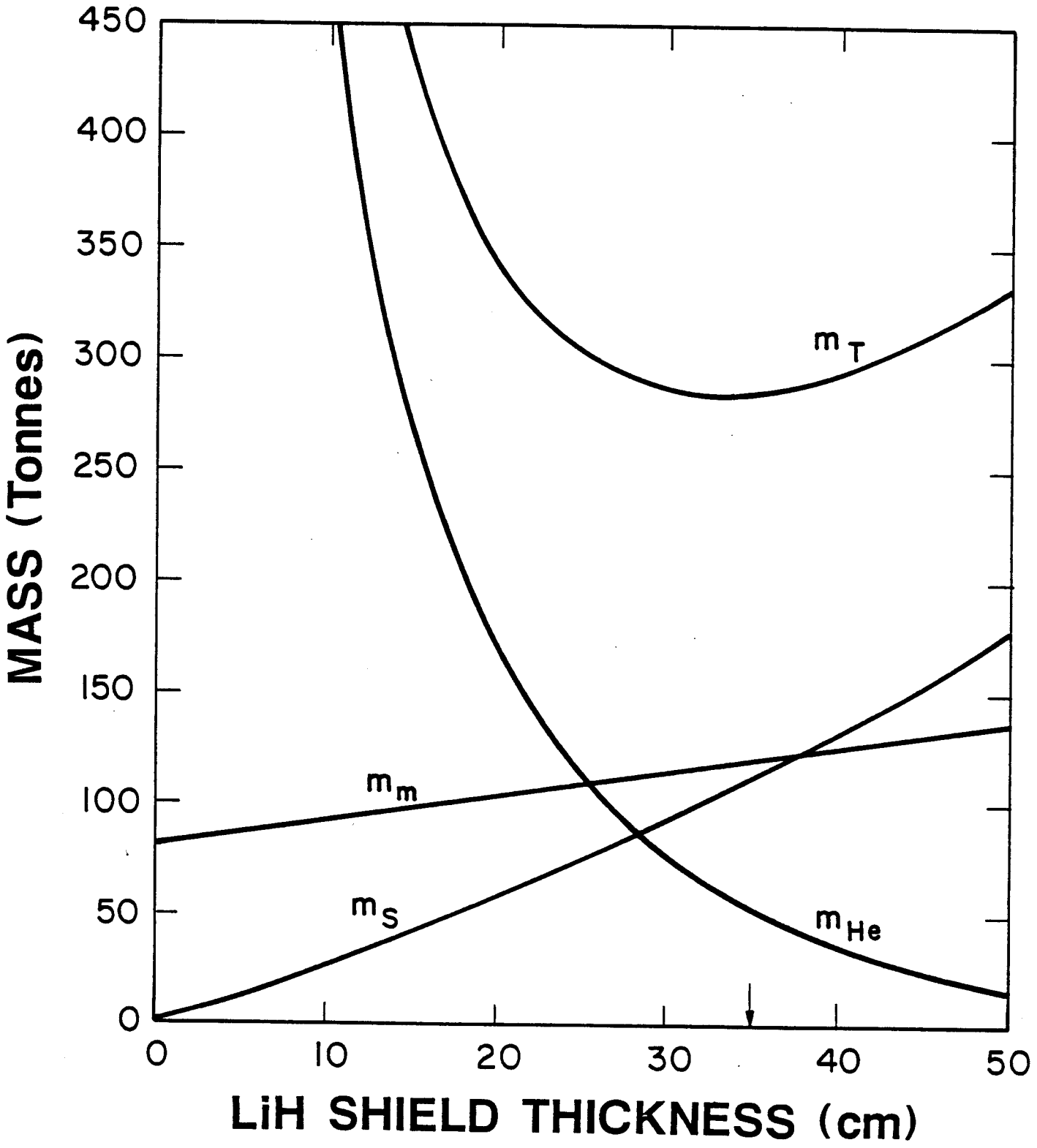

FIGURE 5. Variation of the Mass of the Central Cell Components with LiH Shield Thickness.

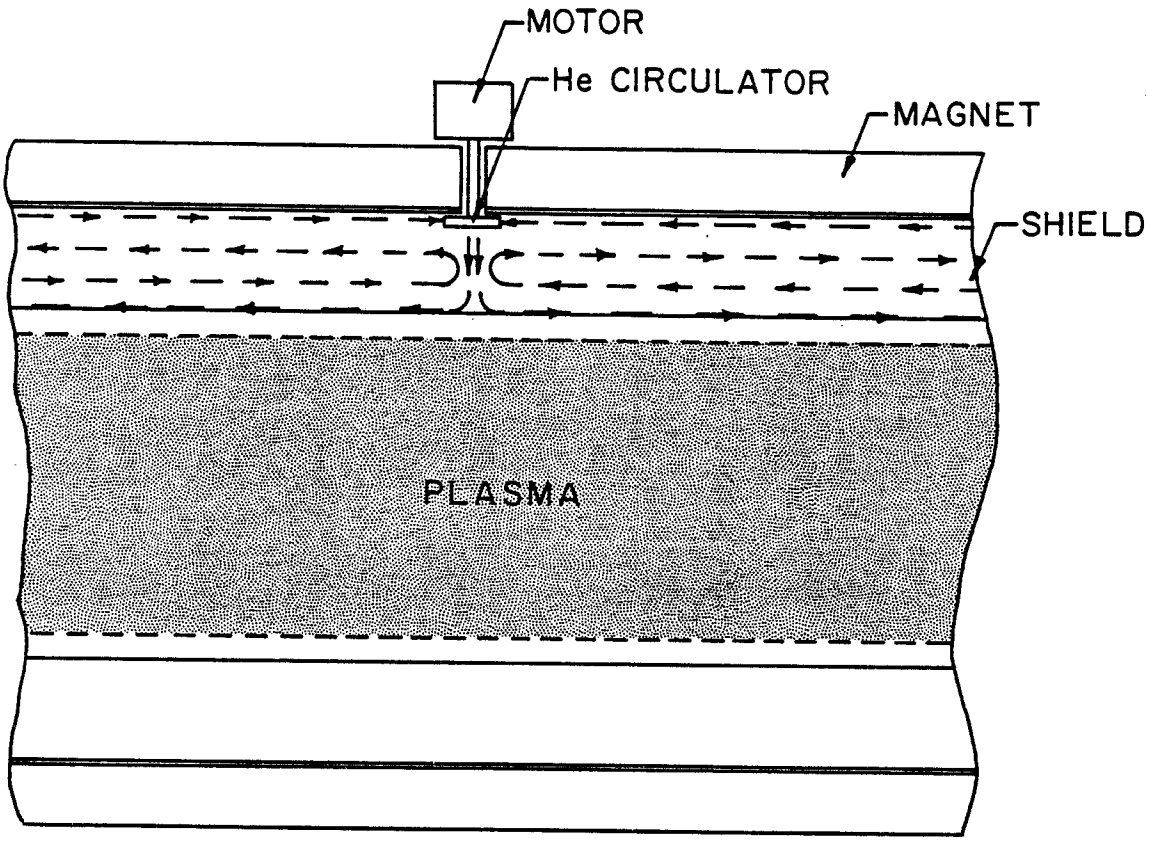

FIGURE 6. A Section of the Central Cell with the Plasma in the Center, Surrounded by the Shield and the Magnet. Arrows Show the Flow Distribution of the He Gas.

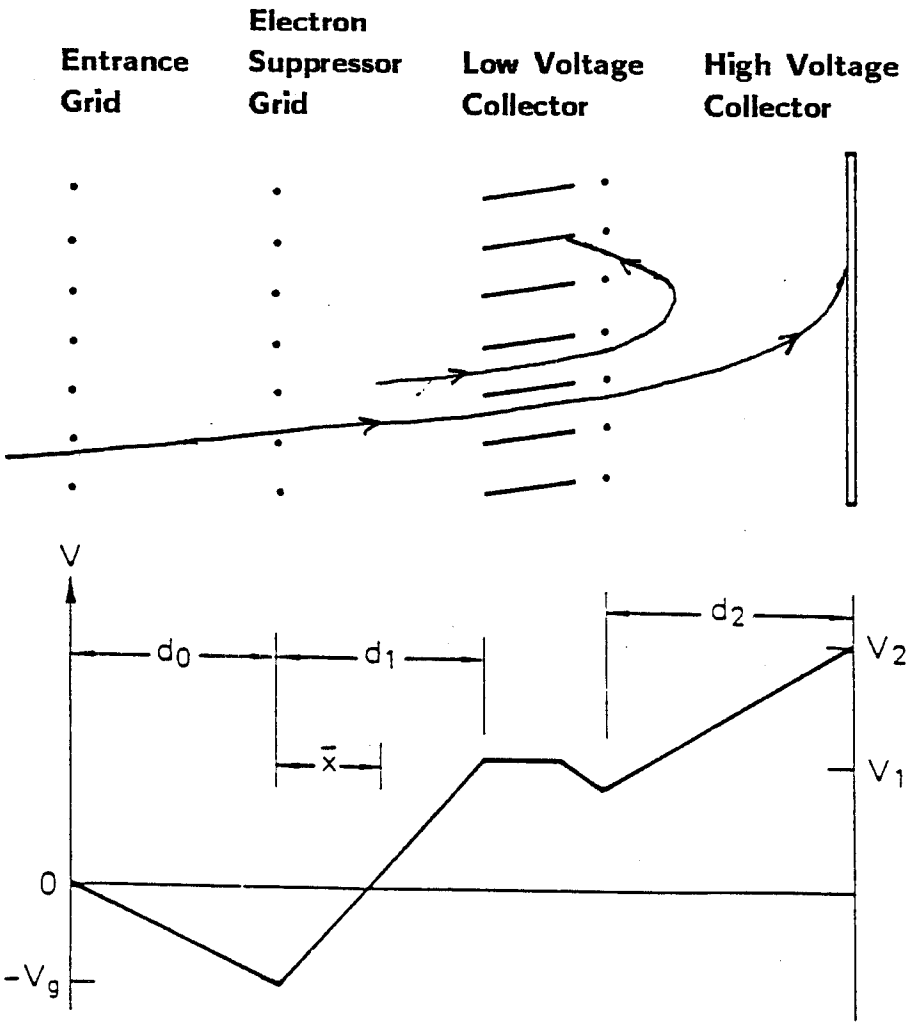

FIGURE 7. Schematic of a 2-Stage Direct Converter.

REFERENCES

Baldwin, D.E. and B.G. Logan (1979) "Improved Tandem Mirror Fusion Reactor," Phys. Rev. Lett. 43, 1318.

Barr, W.L. and R.W. Moir (1983) "Test Results on Plasma Direct Converters," Nucl. Technol./Fusion 3, 98.

Berk, H. et al. (1984) "Stabilization of an Axisymmetric Tandem Mirror Cell by a Hot Plasma Component," Phys. Fluids 27, 2705.

Dawson, J.M. (1981) "Advanced Fusion Reactors," in Fusion, Vol. 1, Part B, E. Teller ed., Academic Press, New York.

El-Guebaly, L.A. (1987) "Magnet Shielding Analysis for SOAR--A Space Reactor," in Proceedings of the 4th Symposium of Space Nuclear Power Systems, held in Albuquerque, NM, 12-16 January 1987.

Englert, G.W. (1962) "Towards Thermonuclear Rocket Propulsion," New Sci. 16, 307, (#16).

Gurol, H., G.W. Shuy, and A.E. Dabiri (1983) "Preliminary Analysis of a Carbon/Carbon Fiber Composite Plasma Direct Converter," Nucl. Technol./ Fusion 4, 1473.

Hershkowitz, N. et al. (1985) "Plasma Potential Control and MHD Stability Experiments in the Phaedrus Tandem Mirror," Tenth International Conference on Plasma Physics and Controlled Nuclear Fusion Research, IAEA, Vienna.

Kesner, J. et al. (1984), "Introduction to Tandem Mirror Physics," PFC/RR-83-35, Massachussetts Institute of Technology, Cambridge, MA.

Kesner, J. et al. (1985), "Axisymmetric Tandem Mirror Stabilized by a Magnetic Limiter," PFC/CP-85-5, Massachussetts Institute of Technology, Cambridge, MA.

Logan, B.G. et al. (1984), "Mirror Advanced Reactor Study," UCRL-53480, Lawrence Livermore National Laboratory, Livermore, CA.

Logan, B.G. et al. (1987), "MINIMARS Conceptual Design Final Report", UCID-20773, Lawrence Livermore National Laboratory, Livermore, CA.

Miley, G.H. (1976) Fusion Energy Conversion, American Nuclear Society, La Grange Park, IL.

Moir, R.W. and W.L. Barr (1973) "'Venetian Blind' Direct Energy Converter for Fusion Reactors," Nucl. Fusion 13, 35.

Perkins, L.J. et al. (1985) "Plasma Engineering for MINIMARS: A Small Commercial Tandem Mirror Reactor with Octopole Plugs," Fusion Technol. 8, 685.

Santarius, J.F. (1987) "Very High Efficiency Fusion Reactor Concept," accepted by Nucl. Fusion (Letter).

Wittenberg, L.J., J.F. Santarius, and G.L. Kulcinski (1986) "Lunar Source of ^{3}He for Commercial Fusion Power," Fusion Technol. 10, 167.

Wittenberg, L.J., J.F. Santarius, and G.L. Kulcinski (1987) "Helium-3 Fusion Fuel Resources for Space Power," in Trans. 4th Symposium on Space Nuclear Power Systems, held in Albuquerque, NM, 12-14 January 1987.